Journal of Solid State Chemistry **166,** 91–103 (2002)
doi:10.1006/jssc.2002.9564, available online at http://www.idealibrary.com on IDEAL®

First Principles Study of H-insertion in MnO_2

D. Balachandran, D. Morgan, and G. Ceder[1]

Department of Materials Science and Engineering, Massachusetts Institute of Technology, 77 Massachusetts Avenue, Room 13-5056, Cambridge, Massachusetts 02139

Received November 28, 2001; in revised form February 11, 2002; accepted February 22, 2002

We present an extensive First Principles study on proton intercalation in the pyrolusite and ramsdellite forms of MnO_2. It is shown that protons are always covalently bonded to an oxygen atom in MnO_2. In ramsdellite, the proton prefers the pyramidal oxygen to the planar coordinated oxygen as that site is farther away from the Mn cations. In both pyrolusite and manganite, the octahedral sites are unstable, but the two local minima on each side of the octahedron are connected by a barrier of only about 25 meV, so that protons may rapidly exchange between these sites. Proton diffusion in pyrolusite occurs by hopping along the 1×1 open tunnels with an activation barrier that increases from about 575 meV at the beginning of discharge to about 1 eV at high H concentration. Diffusion in ramsdellite takes place along the 2×1 open tunnels and occurs with much lower activation energy (respectively, 200 and 400 meV, at low and high H concentrations). Introduction of twinning defects has a large adverse effect on the proton diffusivity. Results indicate that direct H–H interactions are not that significant compared to oxygen-mediated-interactions. Experimental and calculated ramsdellite discharge curves deviate significantly at early stages of the reduction process. The calculations on defected structures indicate that a significant source of this discrepancy may be due to presence of proton-compensated Mn vacancies in real MnO_2, which create local sites with higher discharge potential. The calculations suggest that the ordered phase, observed in experiments at mid-reduction (groutellite, $MnOOH_{0.5}$), is due to the lattice remaining coherent during intercalation. © 2002 Elsevier Science (USA)

1. INTRODUCTION

Electrochemically active γ-MnO_2 is used worldwide as the cathode material in primary alkaline batteries. During discharge of an alkaline cell, Zn is oxidized on the anode and protons are inserted into γ-MnO_2 on the cathode. While considerable empirical optimization of the capacity and insertion rate of H in γ-MnO_2 have been achieved, the detailed relation between the electrochemical properties and the structure of MnO_2 is poorly understood. The control over structure and conditions offered by a First Principles computational approach is, therefore, ideal.

The γ-MnO_2 structure is highly disordered and has been claimed to contain pyrolusite (β-MnO_2), ramsdellite (R-MnO_2), ε-MnO_2 and other polymorphs. Pyrolusite is generally regarded as the most stable polymorph of γ-MnO_2 (1) and its structure may be described as infinite single chains of edge-sharing MnO_6 octahedra, as shown in Fig. 1. Ramsdellite is closely related to the pyrolusite structure except that the single chains of edge-sharing octahedra are now replaced by double chains, as shown in Fig. 2. The ε-MnO_2 structure has been described (2) as a hexagonal closed packing of O^{2-} with Mn^{4+} randomly distributed over half the available octahedral interstices (similar to the NiAs structure), though more recently, ordered versions of ε-MnO_2 have also been proposed (3). Because of the lack of a clear structural description for ε, the work in this paper will be limited to the pyrolusite and ramsdellite polymorphs and defects in them.

The electrochemical properties of MnO_2 electrodes in alkaline aqueous electrolytes are determined by the thermodynamics and kinetics of proton and electron insertion into the MnO_2 host structure. The cathode half-cell reaction can be formally written as

$$MnO_2 + xH^+ + xe^- \rightarrow MnOOH_x. \qquad [1]$$

Remarkably, considerable discussion still exists on the location of protons and their bonding type in MnO_2 as a function of insertion level. Below, we give a brief description of some of the various models that have been proposed for proton location in MnO_2.

Fitzpatrick *et al.* (4) studied hydrogen mobility in two samples of electrolytic manganese dioxide (EMD) (samples R2 and IBA 19) using Fourier transform infrared spectroscopy (FTIR). As they found no discernable changes in the intensity of absorption near the O–H frequency for the initial discharge, it was deduced that protons are delocalized up to $x = 0.63$ (R2) and $x = 0.55$ (IBA 19) in MnO_2H_x.

[1]To whom correspondence should be addressed. E-mail: gceder@mit.edu.

0022-4596/02 $35.00
© 2002 Elsevier Science (USA)
All rights reserved.

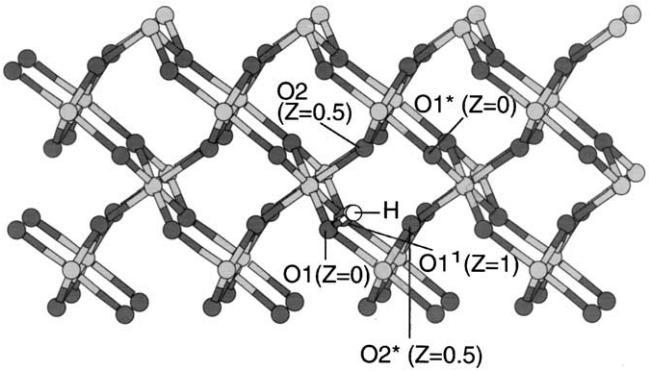

FIG. 1. Illustration of proton location and plausible proton diffusion paths in pyrolusite. Light and dark circles represent Mn and oxygen atoms, respectively. Coordinate z is along the b-axis, into the 1×1 tunnel. A proton is attached to the oxygen marked O1 in the $z = 0$ plane. The various O symbols represent planar-coordinated oxygen atoms in different locations with respect to the protonated O. O^1 is the nearest-neighbor oxygen atom on the same side of the tunnel, translated one lattice parameter along the b-axis. O* represents the oxygen atom across the 1×1 tunnel.

For further discharge, distinct O–H bond formation was observed.

Fillaux *et al.* (5) used inelastic neutron scattering (INS) to study the proton locations in manganite (γ-MnOOH), the end product of pyrolusite reduction (1). From the similarity of the INS spectrum of manganite with those of intermetallic hydrides, Fillaux *et al.* speculated that H is not associated with any particular oxygen atom in manganite, but vibrates around the center of the oxygen octahedron. Based on this premise, the calculated manganite INS spectra were found to closely match those observed experimentally. Furthermore, the observed similarity between the INS spectra of reduced EMD (γ-MnO_2) and natural manganite led Fillaux *et al.* to conclude that both protons in manganite, and protons inserted by reduction into γ-MnO_2, are not covalently bound to the oxygen atoms. The protons are more likely to be found at highly symmetrical positions like the center of the oxygen octahedra.

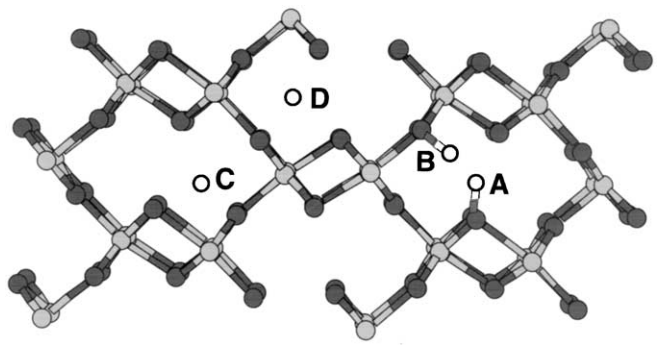

FIG. 2. Plausible locations of protons in ramsdellite. (A) represents a proton site close to a pyramidal oxygen atom; (B) represents a proton site close to a planar oxygen atom; (C) represents a tetrahedral site and (D) represents an octahedral site. Light and dark circles represent Mn and oxygen atoms, respectively.

The validity of Fillaux's results has been questioned in various subsequent papers. Chabre and Pannetier (1) claim that the INS spectra results of Fillaux *et al.* pertain to surface protons, which have a different arrangement than the bulk protons. In addition, the subsequent FTIR results of Kohler *et al.* (6) differ substantially from those of Fillaux *et al.* Kohler *et al.* argue that symmetrical H bonds, as proposed by Fillaux *et al.*, are only observed at O–H $\cdots$ O distances below 2.5 Å while in MnO_2, the O–H $\cdots$ O distance is 2.6 Å.

In their detailed review of the MnO_2–H system, Chabre and Pannetier (1) argue that intercalated protons are always covalently bound to the oxygen atoms in both ramsdellite and pyrolusite. They also state that while pyrolusite contains only one type of oxygen atom, ramsdellite contains two chemically different oxygen atoms (O(pyr) and O(planar), according to their coordination to Mn). Since the two oxygens are at different lattice potentials (O(planar) is less stabilized by the lattice potential), O(pyr) is more likely to be hydroxylated than O(planar).

1.1. Proton Intercalation

Various studies have attempted to describe the reduction process in MnO_2. These differ in whether they describe the process as single- or multi-phase. Even the nature and number of phases involved is unclear.

Brouillet *et al.* (7), using a thin-film electrode and working under galvanostatic and potentiostatic conditions, showed that the kinetics of the MnO_2 reduction could be described by assuming proton diffusion in MnO_2 as the rate-limiting mechanism. The authors concluded that the reduction process to groutite is homogeneous since the potential decreased continuously with the degree of reduction up to one e^-/Mn, and the lattice parameters were observed to expand continuously in the early stage of reduction. Contrary to the results of Brouillet *et al.*, Bell and Huber (8) concluded that reduction of γ-MnO_2 cannot be described by a single Nernst equation up to one e^-/Mn since the slope of the open-circuit voltage (OCV) curves exhibits an abrupt change at about mid-reduction. Based on XRD studies and OCV measurements, Maskell *et al.* (9) proposed a two-step process for electrochemical reduction of γ-MnO_2 up to one e^-/Mn. The reduction proceeds first from MnO_2 to $MnOOH_{0.5}$ and then to MnOOH. This was explained by noting that a Jahn–Teller distortion due to Mn^{3+} occurs at mid-reduction, which was speculated to lead to different locations of the protons in the 2×1 tunnels of the ramsdellite units of γ-MnO_2 before and after mid-reduction.

Kozawa and Yeager (10) observed that after formation of groutite (α-MnOOH), further reduction to Mn^{2+} occurs,

which corresponds to a two-phase equilibrium with a voltage plateau. The mechanism of this step involves the dissolution of Mn^{3+} and Mn^{2+} and precipitation of Mn^{2+} as pyrochroite ($Mn(OH)_2$).

Chabre and Pannetier (1) used results from step potential electrochemical spectroscopy on various γ-MnO_2 samples to argue that the reduction of γ-MnO_2 ideally proceeds in three definite steps. The initial fast reduction process involves surface protons, which account for 5% of the total manganese content. This is followed by the reduction of Mn^{4+} cations located in the ramsdellite units and concomitant proton intercalation into the tunnels of these units. This step occurs in two stages separated by a Jahn–Teller induced structural change, which distorts the shape of the tunnels. The final and slowest step involves the reduction of Mn^{4+} ions located in the pyrolusite units. Chabre and Pannetier also point out that the reduction of γ-MnO_2 follows different paths depending on how far from equilibrium it is carried out. Under conditions near thermodynamic equilibrium, an intermediate phase $MnOOH_{0.5}$ analogous to the mineral groutellite is formed. However, if the reduction is performed under conditions far from equilibrium, the intermediate phase is either not formed or is a highly disordered structure.

Clearly, there currently exists conflicting descriptions of the thermodynamic behavior of protons in γ-MnO_2. In the present work, we demonstrate the use of computational methods to investigate the location, potential and phase diagrams of H in the β- and R-MnO_2 polymorphs. Section 2 describes the computational methodology while proton location and diffusion paths are determined in Section 3 for various MnO_2 and MnOOH polymorphs. The features of the experimental intercalation curve are compared with the calculated intercalation curve for ramsdellite in Section 4, and in Section 5 the effect of Ruetschi defects on the discharge curve is studied. In Section 6, we discuss the relative stability of the groutellite ($MnOOH_{0.5}$) phase. Section 7 contains a final summary and discussion.

2. COMPUTATIONAL METHODOLOGY

To obtain energetic information on proton sites and activation barriers for proton migration in different MnO_2 polymorphs, we use First Principles calculations in the Generalized Gradient Approximation to Density Functional Theory (11). The single-electron wave functions are expanded in a basis of plane waves with kinetic energy less than 405 eV and the atomic cores are represented with ultra-soft pseudopotentials (12), as implemented in the Vienna Ab Initio Simulation Package (VASP) (13, 14). Calculations are converged to within a few meV per $MnOOH_x$ formula unit with respect to k-point sampling in the Brillouin zone. (For a primitive unit cell containing four formula units of MnOOH, we used a $4 \times 4 \times 4$ Monkhorst–Pack mesh centered at Γ.) All calculations were optimized with respect to volume and internal atomic positions, and were calculated with ferromagnetic spin polarization. From previous work (15, 16), we know that antiferromagnetic spin polarization can change the relative stability of polymorphs that are within a range of 10–20 meV of each other. Reaction energies associated with proton insertion are considerably larger. Hence, antiferromagnetic calculations, or paramagnetic extrapolations (15), were not attempted in this work.

Once the low-energy hydrogen sites are identified in a polymorph, the distribution of hydrogen over these sites needs to be calculated at finite temperature. This amounts to determining the MnO_2–MnOOH phase diagram, so techniques from Binary Alloy Theory can be used (17, 18). To obtain thermodynamic information of the MnO_2–MnOOH systems at finite temperature, the material's H configuration is represented by a lattice model that contains all the possible low-energy sites for hydrogen. In this particular system, hydrogen and vacancies are the binary components in the lattice model. The energy of the system as function of the hydrogen distribution is expressed with a lattice model Hamiltonian (usually referred to as a cluster expansion):

$$E = V_0 + \sum_{\alpha} V_\alpha \varphi_\alpha . \qquad [2]$$

The function φ_α is defined as a product of occupation variables $\sigma_i . \sigma_j \ldots \sigma_k$ where the indices $i, j, \ldots k$ correspond to a collection of sites that form a cluster α such as a pair cluster, a triplet cluster, etc. The occupation variable σ_i takes on the value $+1$ (-1) when a hydrogen (vacancy) atom resides on site i. Hence the collection of all cluster functions φ_α fully characterizes the hydrogen distribution of the system, and the set of all coefficients V_α (called ECI or effective cluster interactions) represents the energetics of the system. The ECI are mere expansion coefficients describing the dependence of the energy of the crystal on the H-vacancy configurations and are not to be confused with interatomic potentials commonly used in oxides. In practice, the expansion in Eq. [2] is truncated after a finite number of interactions and these interactions are determined by fitting to the energy of a large number of hydrogen configurations. These energies are calculated with the First Principles energy method. Monte Carlo simulation is used to equilibrate the system at finite temperature. From the hydrogen chemical potential in the Monte Carlo simulation, the open-circuit voltage can be obtained through the well-known Nernst relation (19).

Based on a set of criteria limiting the length of the path and the proximity to Mn ions, possible hydrogen migration paths were identified. For each possible path, the maximum energy along the path (the activated state) was calculated

with Density Functional Theory. The activated state was located with the elastic band method, a well-proven technique to find the minimum energy path between two energetically stable end-points (20). Between four and eight replicas were used in the elastic band approach.

Molecular dynamics (MD) was further used in ramsdellite to check whether any low-energy migration paths had been missed with our selection criteria. Since the Molecular Dynamics is not used to provide quantitative information a simple potential could be used for its energetics. The O–H interaction was modeled using an attractive Morse potential

$$V(\text{O–H}) = D(1 - \exp(-\beta(r - r_0))]^2 \qquad [3]$$

for distances less than 1.5 Å. Beyond that, the O–H interaction was modeled using electrostatic interactions. The parameters for the Morse potential ($D = 7.0525$ eV, $\beta = 2.1986$ Å^{-1}, $r_0 = 0.9845$ Å) were developed by Saul *et al.* (21) using *ab initio* quantum mechanical cluster calculations. The Mn–H interaction was modeled using only electrostatic interactions and the MnO_2 framework was held frozen during the simulation. This model is very approximate but contains enough of the essential physics to be used to qualitatively identify low-energy migration paths. All the calculated numbers presented in this paper were obtained with Density Functional Theory.

3. LOCATION AND MIGRATION OF PROTONS

3.1. Proton Location

Considerable discussion exists on the location of the protons at the beginning of discharge (low concentrations). In order to identify correctly the locations of protons in ramsdellite, pyrolusite, groutite and manganite, the energies of different proton arrangements were evaluated using First Principles energy methods. The calculated bond lengths and crystallographic information are compared to the experimental data in Table 1.

TABLE 1
Comparison of the Experimental and Calculated Structural Parameters for Various MnO_2 and MnOOH Polymorphs

Structure	Experiment	GGA
Pyrolusite(β-MnO_2)		
a, b, c (Å)	4.404, 4.404, 2.876	4.459, 4.459, 2.906
Vol (Å^3), β (deg)	55.781, 90	57.78, 90
D(Mn–O1) (Å)	1.884(4), 1.897(2)	1.9035-9 (4), 1.923 (2)
Ramsdellite(R-MnO_2)		
a, b, c (Å)	9.3231, 4.4531, 2.848	9.425, 4.550, 2.895
Vol (Å^3), β (deg)	118.3, 90	124.14, 90
D(Mn–O1) (Å)	1.815(1), 1.896(2)	1.923 (2), 1.936(1)
D(Mn–O2) (Å)	1.943(2), 1.973(1)	1.911(2), 1.915(1)
Manganite(γ-MnOOH)		
a, b, c (Å)	5.304, 5.277, 5.304	5.309, 5.279, 5.317
Vol (Å^3), β (deg)	135.2, 114.38	137.29, 112.90
D(Mn–O1) (Å)	1.977(1), 1.982(1), 2.337(1)	1.986(1), 1.991(1), 2.319(1)
D(Mn–O2) (Å)	1.881(1), 1.893(1), 2.213(1)	1.947(1), 1.955(1), 2.227(1)
D(H–O1) (Å)	0.98	1.114
D(H–O2) (Å)	1.615	1.360
Groutite(α-MnOOH)		
a, b, c (Å)	10.667,2.871,4.554	10.702, 2.930, 4.558
Vol (Å^3), β (deg)	139.47, 90	142.92, 90
D(Mn–O1) (Å)	1.895(2), 2.174(1)	1.942(2), 2.226(1)
D(Mn–O2) (Å)	1.965(2), 2.338(1)	1.982(2), 2.323(1)
D(H–O1) (Å)	1.818	1.434
D(H–O2) (Å)	0.807	1.083

Note. Experimental data are taken from Refs. (6, 28, 29).

3.1.1. Ramsdellite

There are two symmetry-inequivalent types of oxygen atoms (pyramidal and planar) in the ramsdellite structure, distinguished by the bonding angles they make with their Mn neighbors. Calculations were performed by placing protons at various locations in ramsdellite and allowing the structure to completely relax. Our calculations indicate that the lowest energy for a proton is near a pyramidal oxygen atom. The proton sits about 1 Å from this oxygen atom and is covalently bonded to it (see Fig. 2, point A). The distance from the proton to the pyramidal oxygen across the 2×1 tunnel is about 2.2 Å, so that a weak H-bond is possible. Near a planar oxygen atom, the proton is locally stable (see Fig. 2, point B) but has an energy 140 meV higher than that of a proton bonded to a pyramidal oxygen atom. In the tetrahedral (point C in Fig. 2) and octahedral sites (point D in Fig. 2), the proton is not even locally stable and relaxes to the nearest pyramidal oxygen atom. With a proton placed between two pyramidal oxygen (O) atoms, we find a slight relaxation of the ramsdellite framework: The distance between two pyramidal oxygen atoms across the tunnel shrinks from 3.08 to 2.98 Å.

3.1.2. Pyrolusite

In contrast to ramsdellite, pyrolusite has only one type of oxygen atom (see Table 1). The inserted proton forms a covalent bond with this oxygen, with an O–H distance of 1.06 Å. The distance from the proton to the oxygen across the tunnel is now much smaller than in ramsdellite (1.53 Å) so that a strong hydrogen bond is likely (see Fig. 1). We find that the proton easily hops across the tunnel between the two oxygen atoms, with an activation barrier of ≈ 25 meV. This implies that, although the octahedral site at the center of the 1×1 tunnel is not stable, the thermal motion is such that the average proton position will appear to be at an

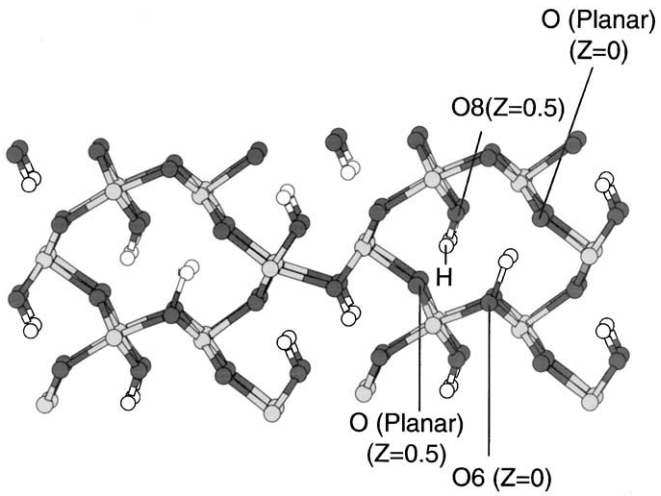

FIG. 3. Illustration of proton location and plausible proton diffusion paths in groutite. The MnO_2 lattice is distorted in groutite due to Jahn–Teller distortion and hydrogen bonding. O6 and O8 represent pyramidal oxygen atoms located at different sites while O(planar) represents a planar oxygen atom. Coordinate z is along the b-axis, into the 2×1 tunnel.

octahedral center. (We believe this may explain the observations of Fillaux *et al.* (5)). In pyrolusite, there is a very large relaxation of the structure on proton insertion. The insertion of a proton makes the O–O distance across the tunnel shrink from 3.23 to 2.59 Å.

3.1.3. Groutite

Groutite (α-MnOOH) is the protonated form of the ramsdellite structure. Compared to ramsdellite, the structure is distorted, primarily due to the Jahn–Teller effect of the Mn^{3+} ions and hydrogen bonding (6). In order to verify the location of protons in groutite, calculations were performed by starting with experimental positions (6) and allowing the structure to completely relax. The calculated structural parameters of groutite, obtained on relaxation, are shown in Table 1. From the table, one can observe that the Mn–O distances in groutite are considerably different from those in ramsdellite, This is likely due to the Jahn–Teller distortions. The structure of groutite is shown in Fig. 3. The calculations show that protons in groutite form a covalent bond with a pyramidal oxygen atom with bond length of 1.08 Å. The distance from the proton to the oxygen across the tunnel is 1.43 Å making a strong hydrogen bond possible. The H geometry and bonding in groutite is different from that in ramsdellite in several ways. In ramsdellite, the oxygen across the tunnel from the proton is another pyramidal oxygen and the proton is too far away from it to form a strong hydrogen bond. In groutite, the original ramsdellite structure has become so distorted that the oxygen across the tunnel from a pyramidal oxygen is a planar oxygen. The discharge proton makes a strong covalent bond with the pyramidal oxygen and is also close enough to form an H-bond with the planar oxygen.

3.1.4. Manganite

Manganite (γ-MnOOH) is the protonated equivalent of the pyrolusite structure and also has a characteristic Mn^{3+} Jahn–Teller distortion (6). Starting from the experimental parameters (6), the manganite structure was fully relaxed in the computations and the resulting structural parameters are shown in Table 1. Similar to the case of groutite, there is a significant difference between the Mn–O distances in manganite and pyrolusite. In manganite (see Fig. 4), the calculated O–H $\cdots$ O distance is only ≈ 2.47 Å. Hence, the bond length of the O–H covalent bond (1.11 Å) is not that different from the O $\cdots$ H hydrogen bond length (1.36 Å). Furthermore, the activation barrier for a proton jump (see Section 3.2) between these two oxygen atoms is very low (< 25 meV). This suggests that the protons in manganite may rapidly move around the octahedral site, which may explain the observations of Fillaux *et al.* (5), who assigned the proton to the octahedral position.

3.2. Proton Migration

Diffusion values for protons in EMD found in the literature range from 10^{-11} to 10^{-16} cm^2/s, although a recent

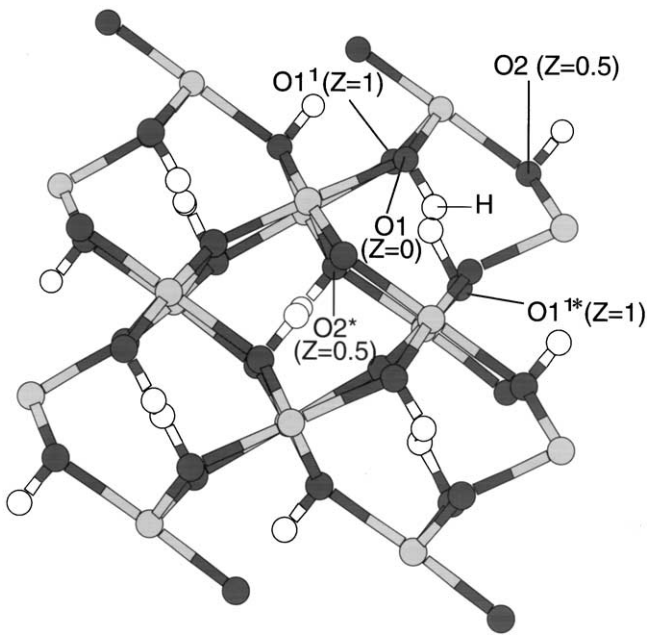

FIG. 4. Illustration of proton location and plausible proton diffusion paths in manganite. The MnO_2 lattice is distorted in manganite due to Jahn–Teller distortion and hydrogen bonding. Coordinate z is along the b-axis, into the 1×1 tunnel. O^1 is the nearest-neighbor oxygen atom on the same side of the tunnel, translated one lattice parameter along the b-axis. O* represents the oxygen atom across the 1×1 tunnel.

assessment of these data by Chabre and Pannetier (1) suggests that the range is 10^{-14}–10^{-16} cm^2/s. This rather slow diffusivity seems to conflict with the idea of delocalized protons (4). In the following sections, the migration path and energy are determined for dilute H and dilute vacancy concentrations in the pyrolusite and ramsdellite polymorphs. To study the effect of twinning disorder the α-PbO_2 structure is also studied, as it can be thought of as the fully twinned version of pyrolusite.

3.2.1. Dilute Proton Concentration

The First Principles calculations were used to calculate the energy barrier for proton migration along different paths in each structure. To limit the number of possible paths that needed to be studied, the following selection criteria were used.

- The path involves hops between proton sites close to an oxygen atom (the proton should form a covalent bond with the oxygen atom).
- The path links proton sites along the same tunnel. It was found that a proton hop between sites located in different tunnels in ramsdellite involves an activation energy barrier $\gg 1$ eV. Hence, these paths were not considered further for elastic band calculations.
- The path involves movement of the proton in the direction of the tunnel. (In pyrolusite, the proton rapidly hops between oxygen atoms located on the same plane perpendicular to the axis of the tunnel (*b*-axis), but this does not constitute diffusion.)

Periodic cells with four MnO_2 formula units were used in all calculations. Hence the charged (discharged) limit was approximated as $MnOOH_{0.25}$ ($MnOOH_{0.75}$). In order to simulate the diffusion of isolated protons or vacancies more accurately, the calculations are done with cell parameters fixed to those of the endmembers (pyrolusite, ramsdellite, groutite or manganite) (see Table 1). However, all internal degrees of freedom were fully relaxed for each supercell.

3.2.1.1. Ramsdellite. The lowest energy path for proton migration consists of hops between pyramidal oxygen ions on opposite sides of the 2×1 tunnel, having a net displacement of $\frac{1}{2}$ the lattice parameter in the tunnel direction. The activation barrier for this hop (O6(pyr) → O8(pyr) in Fig. 5) is about 200 meV. Refer to Fig. 5 for all atom labels (we will also identify the O as pyramidal or planar). Coordinate *z* in the figure is along the *b*-axis, into the tunnel. The results for the other possible paths are as follows:

- The diffusion path O6(pyr) → $O6^1$(pyr) (along the same side of the tunnel) is unstable as H relaxes to the O8 position across the tunnel before reaching the $O6^1$ position.
- The diffusion path O(planar) → O^1(planar) (between planar oxygen atoms) has an energy barrier greater than 1 eV.

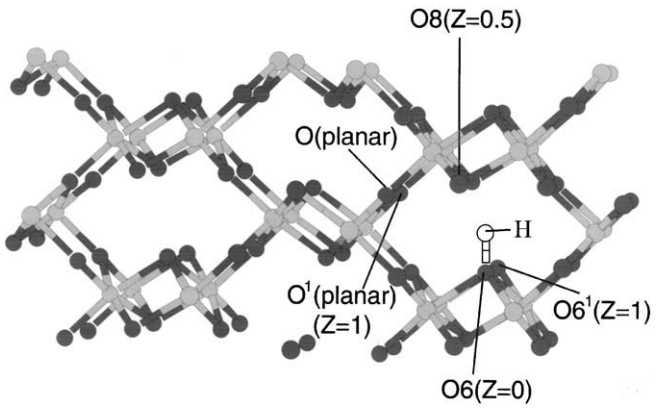

FIG. 5. Illustration of the possible diffusion paths in ramsdellite. O6 and O8 represent pyramidal oxygen atoms while O(planar) represent planar oxygen atoms. Coordinate *z* is along the *b*-axis, into the 2×1 tunnel. The proton is initially on the oxygen labeled O6 in the $z = 0$ plane. O^1 represents its nearest neighbor oxygen atom on the same side of the tunnel, translated one lattice parameter along the *b*-axis.

- The diffusion path O8(pyr) → O(planar) also has an energy barrier greater than 1 eV.

As mentioned earlier, hopping from one tunnel to another was found to have a very high-energy barrier ($\gg 1$ eV).

As the ramsdellite structure is complex, we verified with Molecular Dynamics that no low-energy migration paths were overlooked. Only the path between pyramidal oxygens along different sides of the tunnel showed up in the MD simulation, in agreement with the low activation energy we found for this mechanism. In particular, we found that this migration occurs through what we call a rotation-and-jump mechanism. In the stable configuration, the O(pyr)–H bond does not point towards another pyramidal oxygen. Hence, for the proton to migrate, the O–H bond has to rotate towards another pyramidal oxygen. We find that this rotation can occur easily, while jumping between the oxygen atoms involves crossing a significant energy barrier. A schematic illustration of this hopping method is shown in Fig. 6.

3.2.1.2. Pyrolusite. In pyrolusite, the lowest energy diffusion path was found to be from an oxygen on one side of the tunnel to an oxygen on a neighboring side and displaced by half the unit cell parameter along the tunnel. In Fig. 1, this corresponds to a hop from O1 to O2 (or O2*). The activation energy barrier for this path is 575 meV. The results for the other possible diffusion paths in pyrolusite are as follows:

- The diffusion path O1 → $O1^1$ (along the same side of the 1×1 tunnel) was presumed to be unstable because the proton must hop to either O2 (or O2*) before hopping to an $O1^1$ position.

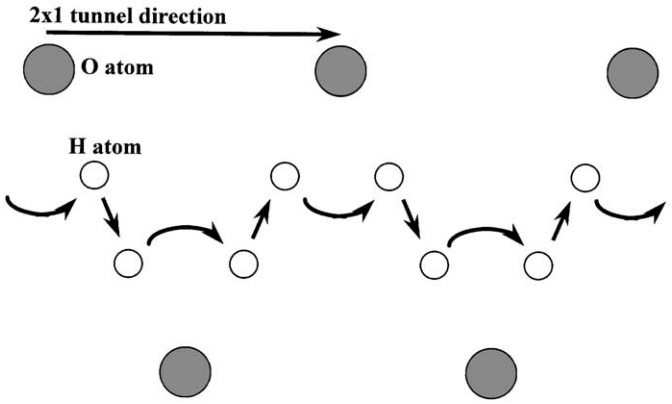

FIG. 6. Schematic illustration of the proton hopping mechanism in ramsdellite. Dark circles represent pyramidal oxygen atoms aligned along the 2×1 tunnels of ramsdellite. Protons jump and rotate between pyramidal oxygen atoms and thus diffuse into the tunnel.

• The barrier for an $O1 \rightarrow O1^*$ hop (across the 1×1 tunnel) is ≈ 25 meV. However, this does not constitute diffusion, as both the oxygen atoms are in the same plane along the tunnel and the proton merely keeps hopping between these two oxygen atoms. This hop occurs with low activation energy because the introduction of protons causes the lattice to relax dramatically, bringing the two oxygen atoms very close together.

The activation barrier is much higher in pyrolusite than in ramsdellite. Hence, De-Wolff defects (1) (i.e., pyrolusite units) in γ-MnO_2 will very likely reduce the electrochemical reactivity by hindering proton diffusion.

3.2.1.3. α-PbO_2. The effect of twinning on the diffusion process was evaluated by studying H migration in the α-PbO_2 structure, the 100% twinned equivalent of the pyrolusite structure (1). Like pyrolusite, this structure has only one type of oxygen atom. Calculations on this structure indicated that the intercalated proton is covalently bonded to an oxygen atom with an O–H distance of 1.12 Å.

Elastic-band calculations indicate that the lowest-energy barrier diffusion path in this structure is a two-step process along the 1×1 tunnel. H initially hops from the O3 position to the O6 position across the tunnel and the barrier is small for this jump (see Fig. 7). It then rotates and jumps further across the tunnel to the O4 position. The activation barrier is ~ 1.2 eV for this jump. The diffusion path $O3 \rightarrow O3^1$ (along the same side of the 1×1 tunnel) is presumed unstable as this distance is 4.8 Å and H hops between several intermediate O atoms before hopping to the $O3^1$ position. From these calculations, it can be observed that twinning the pyrolusite structure qualitatively changes the diffusion path and increases the activation barrier significantly. Therefore, these calculations suggest that twinning will hinder proton diffusion in MnO_2.

3.2.2. Protonated Structures

3.2.2.1. Groutite. Groutite is the protonated form of the ramsdellite structure. In groutite, each of the pyramidal oxygen atoms is involved in a covalent bond with a proton. Proton migration calculations were performed in this structure by introducing a vacancy near a pyramidal oxygen atom and determining the energy barrier for a nearby proton to move into it. The lowest energy path in this structure is analogous to that in ramsdellite and goes along $O6(pyr) \rightarrow O8(pyr)$ (see Fig. 3). The activation barrier for this path is ≈ 400 meV. The path $O(pyr) \rightarrow O(planar)$ is found to be unstable as the proton is not stable near a planar oxygen atom. Thus, in groutite, even though the diffusion path is same as in ramsdellite, the activation barrier is significantly higher.

3.2.2.2. Manganite. Manganite (MnOOH) is the protonated equivalent of the pyrolusite structure. As was done with groutite, diffusion calculations were performed in manganite by the introduction of a vacancy. The calculations indicate that the diffusion path is different in manganite as compared to pyrolusite. In manganite, the $O1 \rightarrow O1^1{}^*$ path is the lowest-energy diffusion path (see Fig. 4). The barrier for this path is ≈ 1 eV. In pyrolusite, this direct path was found to be unstable since the proton relaxes to an intermediate O2 position before reaching the $O1^1{}^*$ position. However, in manganite, this is not possible because there is already a proton attached to the O2 atom in the adjacent tunnel. It is not energetically favorable for two protons to be attached to the same oxygen atom and the intermediate O2 position is no longer a low-energy metastable state.

The activation barrier in manganite is considerably higher than in pyrolusite. This may be due to both structural

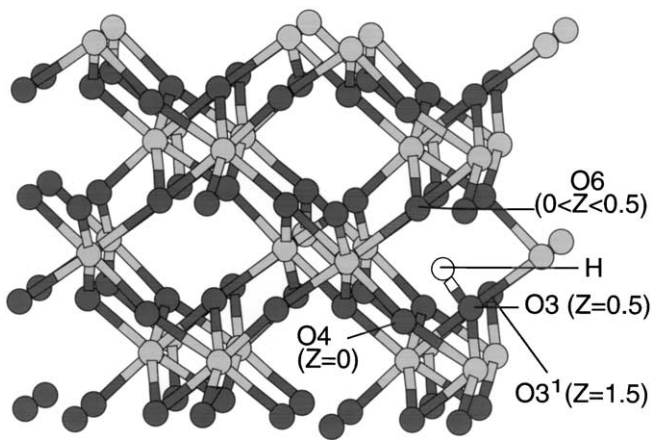

FIG. 7. Illustration of the possible diffusion paths in twinned pyrolusite structure (α-PbO_2). The coordinate z is along the b-axis, into the tunnel. The various O symbols represent different locations of the planar-coordinated oxygen atom. The nearest-neighbor oxygen from the oxygen with the proton (O3) is represented by $O3^1$.

Jahn–Teller distortion and H–O–H interactions. When an oxygen ion is bonded with one hydrogen, the bonding energy for a second hydrogen is considerably lower. This indirect H–O–H interaction significantly affects proton mobility at high H concentrations. When, along the H-hopping path, the proton has to come near an oxygen that already has hydrogen bonded to it (even if it is located on the other side of the tunnel), its energy will go up substantially from the case where there is no hydrogen on the other side of the oxygen. In manganite, the H–O–H interaction causes the O2 position to be unstable for a proton hop and hence the proton diffusion path changes from that found in pyrolusite.

3.2.3. Diffusivity

To estimate diffusion constant from these activation barriers, the following expression for dilute diffusion (tracer diffusion) can be used:

$$D_{\text{tracer}} = a^2 f x_v v^* \exp(-E_a/k_B T), \quad [4]$$

where a is the hop distance, f is the correlation factor, x_v is the concentration of vacancies, E_a is the activation barrier, and v^* is an attempt frequency. To get an estimate for D, we used Eq. (4) with $a = 1$ Å, $f = 1$, $x_v = 1$, and $v^* = 10^{14}$. It must be noted that these values are approximate. The hop lengths vary considerably and some are closer to 3 Å, which would increase D_{tracer} by almost an order of magnitude. Furthermore, a higher-order approximation to f might dramatically lower the value of D_{tracer} for the case when a high concentration is present (end of discharge). Similarly, the exact value of v^* is unknown and might easily vary over an order of magnitude. The chemical diffusion constant is the one of real importance when evaluating the kinetics of discharge, and is related to the tracer diffusivity by the thermodynamic factor F:

$$D_{\text{chem}} = F D_{\text{tracer}}. \quad [5]$$

Although $F \approx 1$ for dilute systems, it has been found in previous calculations that F can vary over 4 orders of magnitude (22). In this system, such large thermodynamic factors are not expected, as the H–H interaction will be shown to be weak in the next section. However, the approximate calculations of $D = D_{\text{tracer}}$ (Table 2) must be taken only as general guideline due to the uncertainty in several parameters. From the results in Table 2, one can observe that the calculated diffusion coefficient for ramsdellite ($D = 4 \times 10^{-6}$ cm^2/s) is much higher than the diffusion coefficients quoted in literature for γ-MnO_2 ($D = 10^{-13}$–10^{-16} cm^2/s) (1). It can also be observed that D is much smaller in pyrolusite and twinned pyrolusite (α-PbO_2 structure). This implies that defects, rather than diffusion through the ramsdellite tunnels, may be rate limiting for proton diffusion in real γ-MnO_2.

TABLE 2
Activation Energy Barriers and Estimated Diffusion Coefficient (D) Values for Various MnO_2 and MnOOH Polymorphs

Structure	Barrier (meV)	D (cm^2/s) $T = 300$ K
MnO_2 polymorphs		
Ramsdellite	200	$\sim 4 \times 10^{-6}$
Pyrolusite	570	$\sim 3 \times 10^{-12}$
Defect Structure		
α-PbO_2	1200	$\sim 7 \times 10^{-23}$
MnOOH polymorphs		
Groutite	400	$\sim 2 \times 10^{-9}$
Manganite	1000	$\sim 2 \times 10^{-19}$

4. INTERCALATION CURVE

4.1. Experimental Intercalation Curve

Various experimental studies have been performed to measure the discharge curve for γ-MnO_2. However, there is a large variation in the intercalation curves published by various authors. This is primarily because the intercalation process in γ-MnO_2 is very dependent on experimental conditions. Electrolyte concentration, rate of reduction, and sample preparation and water content are all features that significantly alter the intercalation curve. However, the following features are normally associated with differential capacity curves of conventional EMD samples under normal reduction conditions (potentials are measured vs Hg/HgO) (1):

- The first peak of the reduction process occurs around $+0.1$ V and is attributed to the reduction of Mn^{4+} ions at the γ-MnO_2 surface. For grains with a size of around 1000 Å, about 5% of manganese cations lie on the surface layer of the grain (1).
- The next peak, between $+50$ and -150 mV, is assigned to the reduction of the ramsdellite units by insertion of protons into its tunnels. The nature and voltage range of ramsdellite reduction depends a lot on the experimental conditions. Under equilibrium condition, two steps rather than one are observed. The first step is a homogeneous reduction process transforming ramsdellite MnO_2 into $MnOOH_{0.5}$ (groutellite) while retaining the shape of the ramsdellite tunnels. The next step, which transforms groutellite (i.e., $MnOOH_{0.5}$) into groutite (α-MnOOH), is accompanied by a collective Jahn–Teller distortion of the [MnO_6] octahedra and the formation of a strong hydrogen-bonding network. This two-step equilibrium reduction of ramsdellite is assumed to correspond to the two peaks observed near equilibrium conditions. Under non-equilibrium conditions, the two steps occur simultaneously and only one peak is observed in the differential capacity curve.

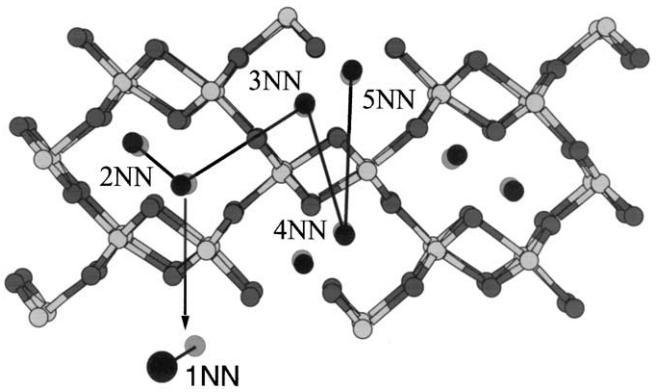

FIG. 8. The clusters used in the cluster expansion to study H insertion.

- A peak is observed between -200 and -400 mV, which corresponds to the reduction of the pyrolusite units in MnO_2.
- Below -430 mV, further reactions take place in concentrated electrolytes, which leads to formation of $Mn(OH)_2$ (pyrochroite).

4.2. Voltage Curve Calculations

The discharge curve for ramsdellite is calculated from the First Principles using the cluster expansion formalism discussed in Section 2. Only proton sites near pyramidal oxygen sites were considered in the model as the other sites were found to have a much higher energy (see the previous section). Hence, octahedral or tetrahedral sites are not considered to take part in the discharge reaction. Groutite has two distinct sites for proton location (near the pyramidal oxygen atoms) within the 2×1 tunnels. Hence, in our calculations, we have assumed these sites to be the H-vacancy lattice in the ramsdellite–groutite system. The various clusters used for the energy parameterization of the H–H interaction energy are shown in Fig. 8. The nearest-neighbor interaction (1NN) is between proton sites connected to pyramidal oxygen along the same side of the tunnel. The pyramidal oxygen atoms involved in this interaction are connected to the same Mn atom. The second-neighbor interaction (2NN) is between proton sites associated with pyramidal oxygen ions on opposite sides of the 2×1 tunnel of groutite. The 3NN, 4NN and 5NN interaction act between proton sites located in different tunnels. In addition to the five pair clusters, a constant and a point cluster were used for the fit. The energies of nine different H-vacancy arrangements, corresponding to different proton intercalation levels in ramsdellite were calculated and used to fit the seven effective interactions. Least-squares procedures (23) were used to optimize the fit and the rms error for the fit was calculated to be 4 meV. From the resulting interaction energies in Table 3, it can be observed that the values of all interactions, of the order of a few meV, are very small. This implies that the effective H–H interactions are weak in this system. In addition, it can also be observed that all interactions are attractive except along the c-axis direction (this is the only interaction where H repel each other). An effective attractive H–H interaction is consistent with the fact that we found all the formation energies in this system to be positive. Formation energy is defined as

$$\Delta E_{\text{form}} = E_{\text{MnOOH}_x} - (1-x)E_{\text{rams}} - xE_{\text{grout}}, \qquad [6]$$

where E_{MnOOH_x} corresponds to the energy of an intermediate $MnOOH_x$ composition while E_{rams} and E_{groutite} represent energy of ramsdellite and groutite, respectively. These results suggest that at low temperature, the system is phase separating, i.e., any intermediate compound is less stable than the mixture of ramsdellite and groutite with equivalent H concentration. This is very surprising since we expect H to repel each other (due to electrostatics) and therefore the system to order. This unusual behavior is probably due to the Jahn–Teller effect and H-bonding. Compositions intermediate between ramsdellite and groutite have a mixture of Jahn–Teller active Mn^{3+} and non Jahn–Teller active Mn^{4+} ions. The distortion around the Mn^{3+} ions causes an elastic strain around the Mn^{4+} ion. Hence, the system prefers to be either fully Mn^{4+} or Mn^{3+}, in which case there is no elastic strain present. In addition, as we will show later, coherency effects can have a significant impact on the ordering behavior of the system.

Using the interaction in Table 3, Monte Carlo simulations were performed at 300 K on a supercell with 4000 H sites. The number of Monte Carlo steps per site was in the range 2000–2500 for each temperature and of those, the first 1000 were excluded from the calculations of thermodynamic quantities to allow for equilibration. From the chemical potential in the Monte Carlo simulation the discharge voltage can be obtained. Figure 9 compares the calculated, experimental, and an ideal solution ($V = V_0 + kT\ln(x/(1-x))$ discharge curves. The experimental data was taken at Energizer Battery Company on a cathode pellet with 50 wt% EMD (balance is graphite) in a flooded

TABLE 3
H–Vacancy Interactions in Ramsdellite

Cluster	Interactions (eV)
Const.	-26.105
Point	2.121
1NN	0.009
2NN	-0.007
3NN	-0.015
4NN	-0.002
5NN	-0.013

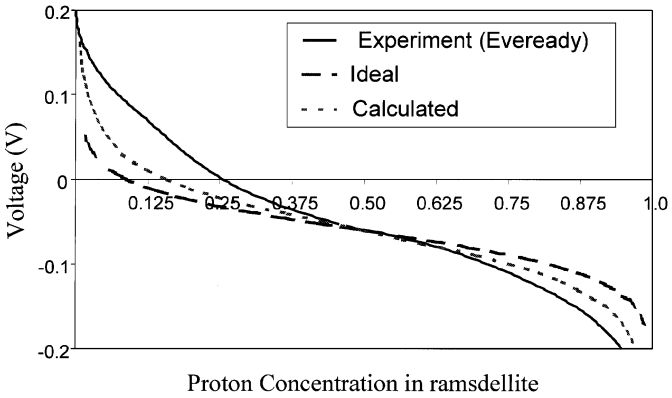

FIG. 9. Experimental, ideal and calculated intercalation curve for ramsdellite voltage vs Hg electrode. The experimental curve was obtained from Energizer Corporation.

electrolyte condition with 37 wt% KOH. Discharge current was 10 mA/g

Since the experimental data, as in most MnO_2 measurements, are obtained on a γ-MnO_2 sample, it is assumed that the initial features of the experimental intercalation curve are due to reduction in ramsdellite units and that reduction in pyrolusite occurs only in the later stages of the reduction process. Therefore, the experimental curve in Fig. 9 has been obtained by removing the last part of the reduction curve and rescaling the remainder. The calculated and ideal solution curves are plotted in such a manner that the potential at half-discharge is the same as that of the experimental curve. The experimental potentials are measured against the Hg reference electrode potential. Even though the zero Kelvin formation energies indicate phase separation between ramsdellite and groutite, the MC results indicate that the entropy of mixing is strong enough to induce solid solution formation at room temperature. On comparing the different curves, it can be observed that the ideal curve is too flat. This is to be expected since the ideal curve assumes no interaction between the protons. The calculated curve fits reasonably well with the experimental curve beyond mid-reduction, but deviates considerably from the experimental curve in the initial stages of the reduction process.

The features of an intercalation curve can be better observed by calculating the differential capacity curve. The experimental differential capacity curve (see Fig. 10) shows a broad peak between a voltage of 0.2 and 0.05. This corresponds to the unusual slope in the experimental discharge curve from $x = 0$ to ≈ 0.2 and is a significant source of the discrepancy between the experimental and calculated curves. This broad experimental peak has been attributed to surface protons, which have not been accounted for in our calculations and this could be a possible reason for the discrepancy. However, it must be noted that irrespective of our calculations, there is a problem in assigning the experimental peak (until $x \approx 0.2$) to surface protons. Surface protons can usually account for only $\sim 5\%$ of the total level of intercalation (1) and hence they cannot completely explain the presence of the peak, which is observed at least until $x \approx 0.2$.

Another possible explanation for the presence of the experimental peak is the effect of Mn defects. In MnO_2, Mn vacancies are compensated by protons and the proton sites near these defects offer a different local environment for incoming protons. Hence, the potential will be different near these defects, which might account for the discrepancy between the experimental and calculated curves at the beginning of discharge. In order to verify this hypothesis, First Principles calculations were performed on ramsdellite with proton compensated Mn vacancies, which are known as Ruetschi defects.

5. RUETSCHI DEFECTS

We will give only a brief description of Ruetschi defects here as they have been described in detail elsewhere (15). EMD generally contains about 4 weight percent of structural water in the crystal structure, which influences not only electrochemical reactivity but also other properties, such as density, electronic conductivity and electrode potential (24–26). The cation vacancy model, proposed by Ruetschi (27), is the most successful model for explaining these properties. According to this model, γ-MnO_2 contains Mn vacancies, compensated by four protons that are attached to the vacancy. First Principles calculations have been performed to ascertain the structural stability of Ruetschi defects in pyrolusite and ramsdellite (15). The calculations indicated that even though pyrolusite is the ground state for stoichiometric MnO_2, ramsdellite is stabil-

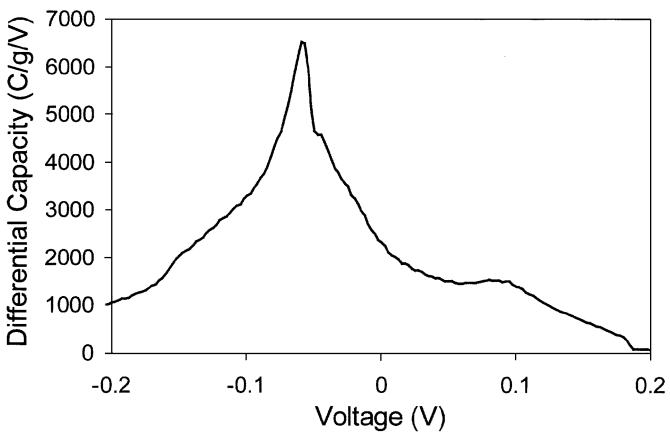

FIG. 10. Experimental differential capacity curve. The latter part of the curve (beyond a proton concentration of 0.8) has been removed in order to focus on the intercalation in ramsdellite.

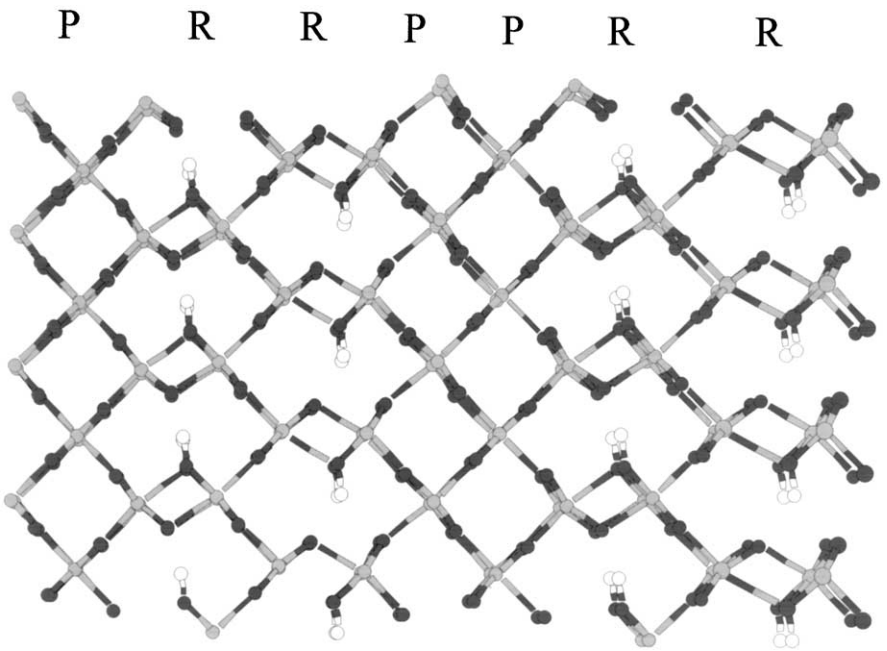

FIG. 11. Illustration of "groutellite" in the $\beta R\beta R$ structure. The structure consists of alternate pyrolusite and ramsdellite slabs. Proton insertion in the ramsdellite slabs is shown.

ized over pyrolusite when Ruetschi defects are present. This implies that Ruetschi defects are more likely to be present in the ramsdellite units of γ-MnO_2. In this work, First Principles calculations were performed to study the effect of Ruetschi defects on the discharge curve of ramsdellite. These Ruetschi defects were previously shown to be key for understanding the large number of polymorphs occurring in MnO_2 (15).

5.1. Effect of Ruetschi Defects on the Intercalation Curve

We believe that the H ions around a Ruetschi defect form a more distortable, less concentrated charge distribution that is less ionic than Mn^{4+} and hence the Ruetschi defect is likely to provide less electrostatic repulsion than a Mn ion. Due to this reduced repulsion, inserted protons may be more stable near a Ruetschi defect than near a Mn ion and the intercalation voltage should be higher when Ruetschi defects are present in ramsdellite. First Principles calculations were performed in ramsdellite to test this hypothesis. Calculations were performed at 12.5% Ruetschi defect concentration with protons placed at sites adjacent to the Ruetschi defects. The calculations indicate that the average voltage between $x = 0$ and 0.125 (x corresponds to $MnOOH_x$) is $\approx$100 meV higher when Ruetschi defects (at conc. of 12.5%) are present in the system. This suggests that protons are more stabilized at sites adjacent to Ruetschi defects, which is in accordance with our reasoning. Hence, Ruetschi defects will increase the potential at the beginning of discharge and may explain the discrepancy at low H concentrations between the experimental (for real γ-MnO_2) and calculated (for perfect ramsdellite) intercalation curves.

6. UNDERSTANDING GROUTELLITE

There is a significant amount of evidence that under certain circumstances, intercalation of ramsdellite leads to an intermediate $H_{0.5}MnO_2$ (groutellite) ordered phase. However, our calculations predict that the intermediate compounds, including groutellite, are not stable. A possible explanation could be that groutellite is stable in a coherent system but unstable in the incoherent system. In a coherent system, the oxygen framework and lattice parameters have to match between different phases, causing strain. In an incoherent system, the oxygen lattice does not match across the boundary and the lattice parameters are allowed to relax freely. In the latter case, the energy of groutellite is 23 meV above that of the ramsdellite–groutite mixture. First Principles calculations were performed to study the effect of coherency on the stability of groutellite.

To approximate the structural energy differences in a coherent system, calculations were performed on ramsdellite, groutite and groutellite with lattice parameters fixed to those of groutellite. Under these conditions, the energy of groutellite is -47 meV per formula unit below that of a mixture of ramsdellite and groutite. These calculations thus indicate that coherency constraints may lead to the stabilization of groutellite. Coherency strains could be

provided by an intergrowth of ramsdellite (R) and pyrolusite (β) units (De Wolff disorder). As the ramsdellite units are reduced by proton insertion, they cannot freely expand since they would be constrained by the unreduced pyrolusite units. To test the hypothesis further, we studied intercalation in a βRβR-intergrowth structure. The βRβR intergrowth has been chosen since it is an idealized representation of the γ-MnO_2 structure, consisting of alternate blocks of pyrolusite and ramsdellite units. When the ramsdellite blocks are reduced in this structure, they are constrained by the surrounding pyrolusite blocks and cannot relax as much as in pure ramsdellite. Hence, the βRβR system acts like a coherent system for proton intercalation. On insertion of protons in the ramsdellite blocks, calculations indicate that when the ramsdellite tunnels are half-filled (see Fig. 11), the formation energy for the structure is -17 meV per formula unit. Since a half-filled ramsdellite structure corresponds to groutellite, these calculations indicate that groutellite will be formed during coherent proton intercalation in a βRβR system.

7. SUMMARY AND DISCUSSION

7.1. Proton Location

There has been considerable discussion over the location of protons in MnO_2. Fitzpatrick *et al.* (4) used FTIR studies on EMD to conclude that protons are delocalized up to a certain discharge level while Fillaux *et al.* (5) used inelastic neutron scattering (INS) studies to conclude that H vibrates at the center of an oxygen octahedron in γ-MnO_2. Our First Principles results indicate that protons are always covalently bonded to an oxygen atom in various MnO_2 and MnOOH polymorphs. This bond is relatively strong and unless a network of similar oxygen atoms exist within short distance of the proton, proton delocalization is unlikely. Furthermore, it was found that in ramsdellite, the protons prefer the pyramidal oxygen atom to the planar-coordinated oxygen atom. We believe that this difference is largely due to the electrostatic interactions between the proton and the Mn ions. This was confirmed by calculating the Madelung field at both sites (1). When connected to the pyramidal oxygen, the proton is further away from Mn ions than when it is connected to the planar oxygen, and it is considerably less stable at the planar site. Calculations suggest that a proton in the octahedral sites is extremely unlikely in ramsdellite and groutite. However, in pyrolusite and manganite, there is a very large relaxation of the structure on proton intercalation. This reduces the O–H $\cdots$ O distance and creates two shallow minima on each side of the octahedral site. Protons can easily hop between them (activation barrier ≈ 25 meV) and hence vibrate around the octahedral sites. This may explain the observations of Fitzpatrick *et al.* (4) and Fillaux *et al.* (5). Such hopping does not constitute diffusion, as it has no component along the tunnel-axis.

7.2. Proton Diffusion

We have found a very wide range of activation barriers for proton diffusion in the common $MnOOH_x$ polymorphs. Ramsdellite has by far the lowest activation barrier for proton diffusion. Diffusion in this polymorph occurs by jumping across the tunnel through the rotation-and-jump mechanism. The large physical space in the 2×1 tunnels, often stated as the reason for high proton transport in ramsdellite, is not directly relevant to the fast proton migration. Rather, it is the topological connectivity of the pyramidal oxygen sites and their relation to the Mn ions that is important. Similar to what we observed when investigating the proton locations, we found that low-energy migration channels are in part determined by electrostatic interaction with Mn cations. Hydrogen atoms prefer not only to be covalently bonded to an oxygen but also to stay as far away as possible from the Mn cations. The activation barrier for proton migration in pyrolusite is considerably higher, which may explain in part why its reduction is usually considered to be slow. Our results suggest that introduction of twinning defects as well as De Wolff disorder can have a large adverse effect on the proton diffusivity in MnO_2. Experimentally, it is found that the kinetics of reduction of γ-MnO_2 slows down towards the end of discharge (1), which has been attributed to reduced proton diffusivity. Our results confirm that this may be the case. Activation energies in the reduced polymorphs are considerably higher than in the unreduced polymorphs, for both ramsdellite and pyrolusite. We believe this increase to be due to structural changes induced by Jahn–Teller distortions and interaction between the H atoms. Interestingly, our cluster expansion results suggest that direct H–H interactions are very weak for this system; instead, calculations in manganite indicate that the oxygen mediated indirect H–O–H interactions play a more significant role. Proton diffusion in manganite is along a path different from that of pyrolusite. Diffusion in pyrolusite occurs through a proton hop between neighboring oxygen atoms along the 1×1 tunnel. However, this diffusion path is unstable in manganite since the neighboring oxygen atom in manganite is already bonded to a proton on the other side of the tunnel and hence the proton has to traverse further to hop to an oxygen atom with no prior protons bonded to it. Thus, the H–O–H interaction is caused by one H taking up the oxygen bonding potential that another H needs to allow easy transport. This somewhat novel mechanism for protons impeding each other's transport needs further investigation to confirm its importance.

7.3. Voltage Curve

Intercalation calculations on the ramsdellite–groutite system indicate that H–vacancy interactions are weak and

repel each other in the system. This leads to a phase separating system below $T = 200$ K. At room temperature, the entropy of mixing is strong enough to induce solid solution formation. Real γ-MnO_2 is probably better approximated as ramsdellite with some other phases that impose coherency strains on the ramsdellite units. Calculations suggest that this coherency strain can have a significant impact on the ordering behavior of the system. If the system is allowed to be incoherent during intercalation, groutellite is unlikely to be formed. The $MnOOH_x$ system will behave as a solid solution between ramsdellite (MnO_2) and groutite (MnOOH). However, if the system is constrained to be coherent, the intermediate groutellite ($MnOOH_{0.5}$) phase is likely to be formed.

Comparison of a calculated discharge curve for perfect ramsdellite and experimental discharge curves indicates a discrepancy between the two curves at low reduction levels. Experimental differential capacity curves show a broad peak until $x \approx 0.2$ (x corresponds to $MnOOH_x$), which is not observed in calculations on pure ramsdellite. However, intercalation calculations performed on ramsdellite with proton-compensated Mn vacancies (i.e., Ruetschi defects) indicate that intercalated protons are more stable near these defects (and hence reduce at higher potential). We believe that the discrepancy between the calculated and experimental intercalation curves in Fig. 9 is due to the presence of Ruetschi defects in the experimental samples. These defects are probably the true source of the broad peaks in the differential capacity curve from $x = 0$ to ≈ 0.2. This peak has been attributed to surface protons, but surface protons are generally too small a fraction of the capacity to affect the system up to a discharge state of $x \approx 0.2$. Thus, Ruetschi defects play a significant role in the intercalation process of γ-MnO_2.

ACKNOWLEDGMENTS

This work was performed with the support of Energizer Battery Corporation. The authors gratefully acknowledge discussions held with Dr. Paula Hughes, Dr. Huang Weiwei, Dr. Aron Newman, Dr. Scott Dunn, Dr. Alan Ayers, Dr. Frank Feddrix, and Prof. Art Heuer.

REFERENCES

1. Y. Chabre and J. Pannetier, *Prog. Solid State Chem.* **23,** 1 (1995).
2. P. M. De Wolff, J. W. Visser, R. Giovanoli, and R. Brutsch, *Chimia* **32,** 257 (1978).
3. A. H. Heuer, A. He, P. Hughes, and F. Feddrix, IBA 2000 Manganese Oxide Symposium, Argonne, IL, May 9–12, 2000.
4. J. Fitzpatrick, L. A. H. Maclean, D. A. J. Swinkels, and F. L. Tye, *J. Appl. Electrochem.* **27,** 243 (1997).
5. F. Fillaux, C. H. Cachet, H. Ouboumour, J. Tomkinson, C. Levy-Clement, and L. T. Yu, *J. Electrochem. Soc.* **140,** 585 (1993).
6. T. Kohler, T. Armbruster, and E. Libowitzky, *J. Solid State Chem.* **133,** 486 (1997).
7. P. Brouillet, A. Grund, F. Jolas, and R. Mellet, *C. R. Acad. Sci. Paris* **257,** 3390 (1963).
8. G. S. Bell and R. Huber, *J. Electrochem. Soc.* **111,** 1 (1964).
9. W. C. Maskell, J. E. A. Shaw, and F. L. Tye, *Electrochim. Acta* **26,** 1403 (1981).
10. A. Kozawa and J. F. Yeager, *J. Electrochem. Soc.* **112,** 959 (1965).
11. P. Hohenberg and W. Kohn, *Phys. Rev. B* **136,** 864 (1964).
12. D. Vanderbilt, *Phys. Rev. B* **41,** 7892 (1990).
13. G. Kresse and J. Furthmuller, *Comput. Mater. Sci.* **6,** 15 (1996).
14. G. Kresse and J. Hafner, *Phys. Rev. B* **49,** 14 251 (1994).
15. D. Balchandran, D. Morgan, A. Van de Walle, and G. Ceder, in preparation.
16. S. K. Mishra and G. Ceder, *Phys. Rev. B* **56,** 6120 (1999).
17. G. Ceder, and A. Van der Ven, *Electrochim. Acta* **45,** 131 (1999)
18. D. de Fontaine, *Solid State Phys.* **47,** 33 (1994).
19. M. K. Aydinol, A. F. Kohan, G. Ceder, K. Cho, and J. Joannopoulos, *Phys. Rev. B* **56,** (1997).
20. G. Mills, H. Jonsson, and G. K. Schenter, *Surf. Sci.* **324,** 305 (1995).
21. P. Saul, C. R. A. Catlow, and J. Kendrick, *Philos. Mag. B.* **51,** 107 (1985).
22. A. Van der Ven and G. Ceder, *Electrochem. Solid State Lett.* **3,** 301–304 (2000).
23. J. W. D. Connolly and A. R. Williams, *Phys. Rev. B* **27,** 5169 (1983).
24. A. Kozawa, *J. Electrochem. Soc.* **106,** 79 (1959).
25. A. J. Brown, F. L. Tye, and L. L. Wood, *J. Electroanal. Chem.* **122,** 337 (1981).
26. E. Preisler, *J. Appl. Electrochem.* **6,** 311 (1976).
27. P. Ruetschi, *J. Electrochem. Soc.* **131,** 2737 (1984).
28. A. A. Bolzan, C. Fong, B. J. Kennedy, and C. J. Howard, *Aust. J. Chem.* **46,** 939 (1993).
29. C. Fong, B. J. Kennedy, and M. M. Elcombe, *Z. Fuer Kristallogr.* **209,** 941 (1994).